energies

MDPI

Article

Performance and Efficiency Evaluation of a Secondary Loop Integrated Thermal Management System with a Multi-Port Valve for Electric Vehicles

Jaehyun Bae [1], Jinwon Yun [2,*] and Jaeyoung Han [1,3,4,*]

[1] Department of Mechanical Engineering, Kongju National University, 1223-24, Cheonan-daero, Seobuk-gu, Cheonan-si 31080, Chungcheongnam-do, Republic of Korea; a20240109@smail.kongju.ac.kr
[2] Department of Energy and Mineral Resources Engineering, Dong-A University, 37, Nakdong-daero 550beon-gil, Saha-gu, Busan 49315, Republic of Korea
[3] Department of Future Automotive Engineering, Kongju National University, 1223-24, Cheonan-daero, Seobuk-gu, Cheonan-si 31080, Chungcheongnam-do, Republic of Korea
[4] Institute of Green Car Technology, Kongju National University, 1223-24, Cheonan-daero, Seobuk-gu, Cheonan-si 31080, Chungcheongnam-do, Republic of Korea
* Correspondence: jwyun@dau.ac.kr (J.Y.); hjyt11@kongju.ac.kr (J.H.); Tel.: +82-51-200-7765 (J.Y.); +82-41-521-9241 (J.H.)

Abstract: Recently, battery electric vehicles (BEVs) have faced various technical challenges, such as reduced driving range due to ambient temperature, slow charging speeds, fire risks, and environmental regulations. This numerical study proposes an integrated thermal management system (ITMS) utilizing R290 refrigerant and a 14-way valve to address these issues, proactively meeting future environmental regulations, simplifying the system, and improving efficiency. The performance evaluation was conducted under high-load operating conditions, including driving and fast charging in various environmental conditions of 35 °C and −10 °C. As a result, the driving efficiency was 4.82 km/kWh in high-temperature conditions (35 °C) and 4.69 km/kWh in low-temperature conditions (−10 °C), which demonstrated higher efficiency than the Octovalve-ITMS applied to the Tesla Model Y. Furthermore, in fast charging tests, the high voltage battery was charged from a 10% to a 90% state of charge in 26 min at 35 °C and in 31 min at −10 °C, outperforming the Octovalve-ITMS-equipped Tesla Model Y's fast charging time of 27 min under moderate ambient conditions. This result highlights the superior fast-charging performance of the 14-way valve-based ITMS, even under high cooling load conditions.

Keywords: battery electric vehicle; integrated thermal management system; multi-port valve; secondary loop; heat pump system; HVAC system

Citation: Bae, J.; Yun, J.; Han, J. Performance and Efficiency Evaluation of a Secondary Loop Integrated Thermal Management System with a Multi-Port Valve for Electric Vehicles. *Energies* **2024**, *17*, 5729. https://doi.org/10.3390/en17225729

Academic Editors: Deqiang He, Zhenzhen Jin and Dechen Yao

Received: 21 October 2024
Revised: 11 November 2024
Accepted: 12 November 2024
Published: 15 November 2024

1. Introduction

1.1. Research Background

The global issues of energy depletion and environmental pollution are accelerating the need for BEVs as an alternative to internal combustion engine vehicles (ICEVs) [1,2]. As a representative eco-friendly vehicle, BEVs produce no emissions during operation and offer high energy efficiency in their powertrain [3,4]. However, short driving ranges and long charging times remain key technical challenges limiting the widespread adoption of BEVs [5–7].

To address these issues, methods such as increasing the capacity and energy density of the high voltage battery (HVB) or enhancing the charging power can be considered; however, these approaches may raise manufacturing costs for BEVs and increase the risk of fire due to HVB overheating [8,9]. Therefore, to extend the driving range of BEVs and improve driving performance, it is essential to enhance the efficiency of the entire vehicle system. The BEV powertrain already has significant efficiency, leaving little room for

further improvement [3,4]. However, the thermal management system (TMS) of BEVs can cause a variance of 16–46% in driving range when the HVAC system is used for cabin heating while driving in cold climates [10]. This shows that TMS design has a significant impact on the driving range of BEVs and indicates great potential for energy savings.

BEV-TMS requires more complex thermal management than ICEV-TMS. The engine, which is the main target of thermal management in ICEV-TMS, operates at temperatures between 80 and 120 °C, which are higher than ambient temperatures [11–13]. Therefore, in hot climates, engine cooling can utilize ambient air, while cabin cooling can be achieved using the air conditioning system. Additionally, in cold climates, transferring the substantial heat generated by the engine to the cabin can facilitate efficient heating. However, BEV-TMS must be designed to meet the thermal management requirements of the HVB, (power electronics) PE module, and cabin. The optimal operating temperature range for the HVB is 15–40 °C [14]. Thus, in hot climates, a refrigerant system is required to cool the battery to a temperature lower than the outside air [15–19], while in cold climates, the HVB must be heated quickly [20–23]. The optimal operating temperature range for the PE module is −40 to 90 °C [24], and while its wide temperature range results in lower thermal loads, heat storage and dissipation must be managed smoothly. Additionally, the cabin must meet the comfort zone requirements outlined by ASHRAE Standard 55 [25] and ISO 7730 [26] to ensure passenger comfort. To efficiently manage these diverse thermal management demands, it is necessary to design a thermal management system capable of integrating thermal flow between heat sources.

BEV-TMS uses refrigerants for cabin thermal management and efficient thermal flow between heat sources. Refrigerants, with their low condensation point, high evaporation point, and high latent heat, are fluids capable of effective heat transfer. However, refrigerants are subject to environmental regulations, particularly due to concerns over global warming potential (GWP) [27] and perfluoroalkyl and polyfluoroalkyl substances (PFAS) [28]. As a result, the use of traditional refrigerants such as R134a, R1234yf, R32, and R410a has been restricted. In this context, alternative refrigerants such as R290 and R744 have gained attention as next-generation options for BEV-TMS [29]. R290 offers high latent heat and operates at pressures similar to conventional refrigerant systems, making it well-suited for BEV-TMS [30,31]. Additionally, R290 is not subject to current environmental regulations, which positions it as a key component in future BEV thermal management systems. However, R290 is highly flammable, necessitating the use of an indirect heat pump system to mitigate safety concerns [32]. Implementing R290 may require structural changes at the system level to ensure safe operation. On the other hand, R744, although environmentally friendly with a low GWP, performs well only at high temperatures and is less effective at low temperatures, which limits its versatility in BEV-TMS applications [30,31,33]. Furthermore, R744 requires a significantly higher operating pressure of 70–120 bar compared to conventional systems, resulting in increased manufacturing costs due to the need for reinforced system designs [30,33]. Unlike R290, applying R744 necessitates not only structural modifications but also adjustments to individual components across the system to handle the high pressures and durability requirements. Consequently, while R744 and R290 are both promising refrigerants for future thermal management, R290's compatibility with existing pressure levels and exemption from environmental regulations make it a more practical choice for next-generation BEV-TMS.

The development of an optimized TMS is urgently needed to improve the driving range of BEVs and to comply with environmental regulations. Therefore, it is essential to develop a TMS that can operate with high performance and efficiency by using refrigerants that are not subject to environmental regulations, while optimizing thermal flow between heat sources in BEVs.

1.2. Research Survey

Previous research on BEV-TMS has mostly focused on independent thermal management methods or has been limited to specific conditions. Wang et al. [34] optimized an

air-cooled battery thermal management system (BTMS) by placing parallel plates between the cells, which resulted in a 6.26% reduction in maximum temperature compared to a typical Z-type BTMS. However, air-cooled BTMS is not suitable for cooling high-density batteries due to the low heat capacity of air and its poor cooling performance in high-temperature environments. Akbarzadeh et al. [35] compared air-cooled and liquid-cooled BTMS. The study showed that, when cooling with 0.5 W of power, the liquid-cooled system could reduce the battery cell temperature by 3 °C compared to the air-cooled system. However, since this study was limited to BTMS, it did not assess the overall performance and efficiency of the entire TMS. Shen et al. [36] demonstrated the thermal management capability of a TMS that considered both the HVB and cabin cooling loads. However, the impact of the PE module's thermal load on the TMS was not considered. These independent thermal management approaches focus on specific thermal management elements, making it difficult to optimize the performance of the overall system.

Singirikonda et al. [37] focused on a TMS designed for the entire system, demonstrating effective thermal management for the HVB, PE module, and cabin. However, they relied solely on a positive temperature coefficient (PTC) heater as the heat source for cabin heating and did not consider the overall energy efficiency of the vehicle. Leighton et al. [38], Tian et al. [39], and Shelly et al. [40] showed that applying a heat pump to the BEV thermal management system and integrating the thermal behavior between heat sources could improve driving range by 9%. Guo et al. [41] developed a thermal management system that considered the thermal loads of the HVB, PE module, and cabin, efficiently managing the overall thermal flow of the BEV. However, their analysis focused solely on thermal management performance in cold climate driving conditions. Additionally, while these thermal management methods have the potential to improve efficiency, they may also increase system complexity.

Tesla applied the Octovalve and a heat pump to the Model Y, developing an ITMS that can smoothly manage the thermal flow throughout the entire system [42,43]. While the Octovalve-ITMS achieved both system simplification and improved thermal management efficiency, it uses refrigerants like R134a and R1234yf, which are subject to PFAS regulations and will be prohibited in the future. Therefore, with the need for refrigerants that comply with environmental regulations while remaining efficient, R290 has emerged as an optimized refrigerant for next-generation BEV-TMS due to its latent heat properties and suitable operating pressure. However, R290 is highly flammable and cannot be applied to the Octovalve-ITMS, which uses a direct heat pump system. Thus, to address this issue, the development of an ITMS using an indirect heat pump system is required.

1.3. Motivation and Novelty

According to previous studies, integrating thermal management elements using a heat pump system can improve the driving range of BEVs. However, research on ITMS lacks comprehensive vehicle-level analysis, and further studies are needed in this area. Additionally, many existing studies have focused on analyzing driving conditions in specific climates, underscoring the need for research that reflects various climate and operating conditions. Moreover, while studies on the Octovalve-ITMS have aimed to enhance thermal management efficiency and reduce system complexity, the development of a new ITMS has become essential due to environmental regulations on refrigerants.

Therefore, this numerical study aims to develop an ITMS that can comprehensively manage the thermal behavior of elements requiring thermal management in BEVs, comply with environmental regulations, and achieve system simplification. Additionally, to evaluate the developed ITMS under various high-load operating conditions, simulations of driving and fast charging in both hot and cold climates will be conducted to assess its performance.

The main novelties of this study are as follows:

1. Develop a multi-port thermal management system that adopts the R290 refrigerant and an indirect heat pump system, considering environmental regulations, system efficiency, and flame propagation in the cabin.
2. Apply a 14-way valve to integrate and manage complex thermal flows between various heat sources, increasing system efficiency while reducing complexity.
3. Develop four high-load testing environments for the following: driving in hot climates, driving in cold climates, fast charging in hot climates, and fast charging in cold climates. Evaluate the thermal management performance of the designed 14-way valve-based ITMS using these conditions.

In conclusion, this study develops an R290-applied, 14-way valve-based ITMS, performing integrated thermal management under various climate and operating conditions to analyze system performance and efficiency while proposing a method to reduce complexity.

2. Materials and Methods

2.1. Vehicle Component Modeling

In this study, a vehicle model was applied to analyze the performance and efficiency of the BEV-ITMS at the vehicle level. The vehicle model consists of the HVB, PE module, reducer, vehicle dynamics, vehicle control unit (VCU), driver, low-voltage battery (LVB), and low-voltage electrical components. Through this, the thermal and energy loads generated during vehicle operation are comprehensively predicted.

2.1.1. HVB Modeling

The HVB model is of the NMC type and is a key component that supplies all the energy required by the BEV. It is highly sensitive to operating temperature, making it essential to predict its heat generation accurately. Therefore, the heat generation of the HVB is calculated using the Bernardi heat generation model based on charging and discharging data [44].

$$\dot{Q}_{HVB} = {I_{HVB}}^2 R_{HVB} + I_{HVB} T_{HVB} dU_0/dT_{HVB} \quad (1)$$

In this context, I_{HVB} represents the charging/discharging current, and dU_0/dT_{HVB} denotes the entropy coefficient [45].

Based on the calculated heat generation of the HVB, the temperature of the HVB cells can be predicted.

$$\frac{dT_{HVB,cell}}{dt} = \frac{\dot{Q}_{HVB} - \dot{Q}_{HVB,cell-case,cond}}{m_{HVB,cell} C_{p,HVB,cell}} \quad (2)$$

The operating temperature of the HVB, as shown in Figure 1, significantly affects its performance and efficiency [46,47]. As the operating temperature of the HVB increases, its internal resistance decreases, which leads to improved HVB efficiency. However, if the operating temperature becomes excessively high, it can result in overcurrent flow, potentially leading to thermal runaway.

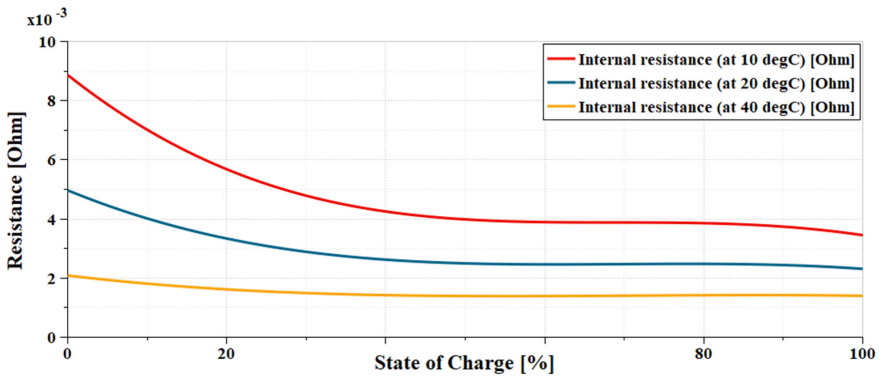

Figure 1. HVB internal resistance across various temperatures.

2.1.2. PE Module Modeling

The PE module consists of a driving motor, inverter, and DC-DC converter, and is designed to facilitate energy conversion between mechanical and electrical energy. All losses generated during this energy conversion process are converted into heat. The total heat generation of the PE module can be calculated as the sum of the heat generated by each component [48].

$$\dot{Q}_{PE} = \dot{Q}_{motor} + \dot{Q}_{inverter} + \dot{Q}_{converter} \tag{3}$$

Here, $\dot{Q}_{motor}$, $\dot{Q}_{inverter}$, and $\dot{Q}_{converter}$ represent the heat generation of the driving motor, inverter, and DC-DC converter, respectively.

The heat generation of each component is defined as follows, and $\dot{Q}_{motor}$ is distinguished based on the operating mode: either motor mode or generator mode.

$$\begin{aligned} \dot{Q}_{inverter} &= (1 - \eta_{inverter}) P_{inverter} \\ \dot{Q}_{converter} &= (1 - \eta_{converter}) P_{converter} \\ \dot{Q}_{motor} &= (1 - \eta_{motor}) |P_{mec}| \ (in\ generator\ mode) \\ \dot{Q}_{motor} &= \left(\frac{1}{\eta_{motor}} - 1 \right) |P_{mec}| \ (in\ motor\ mode) \end{aligned} \tag{4}$$

Here, η_{motor} represents the efficiency, which is defined as P_{mec}/P_{elec} in motor mode and P_{elec}/P_{mec} in generator mode.

Based on the calculated heat generation of the PE module, the temperature of the PE module can be predicted.

$$\frac{dT_{PE}}{dt} = \frac{\dot{Q}_{PE} - \dot{Q}_{PE-cool,conv}}{m_{PE} C_{p,PE}} \tag{5}$$

2.1.3. Powertrain Modeling

The developed powertrain model was constructed to evaluate the 14-way valve-based ITMS at the vehicle level. The powertrain specifications were based on the Tesla Model Y (long range, AWD, 2020), and as presented in Table 1, the total vehicle weight is 2056 kg and the total capacity of the HVB is 75 kWh.

Table 1. Vehicle performance and specifications.

Parameters	Value	Unit
total weight	2056	kg
maximum continuous torque	front (230) rear (247)	Nm
maximum continuous speed	front (12,000) rear (12,000)	rev/min
maximum braking torque	4000	Nm
HVB capacity	75	kWh
number of HVB cells	4416 (46P96S)	-
reduction gear ratio	front (9.0363) rear (9.0363)	-
drag coefficient	0.23	-
rolling resistance coefficient	0.01	-
vehicle front area	2.91	m^2
wheel rim diameter	19	inch

2.2. ITMS Component Modeling

In this study, a model of the ITMS components was developed to evaluate the 14-way valve-based ITMS. The developed ITMS is designed around the 14-way valve and refrigerant system to comprehensively manage various thermal loads within the vehicle, enabling efficient control of the flow and thermal behavior of multiple working fluids. This section explains the components of the 14-way valve-based ITMS and each corresponding model.

2.2.1. System Overview

The developed ITMS, as shown in Figure 2, consists of a refrigerant module, coolant module, and blower case. In particular, the 14-way valve, the key component of this study, is an innovative part designed to significantly reduce the complexity of conventional ITMS through rotation and to flexibly control fluid flow. By effectively controlling the thermal flow between refrigerant, coolant, and air depending on various operating modes, it enhances system efficiency.

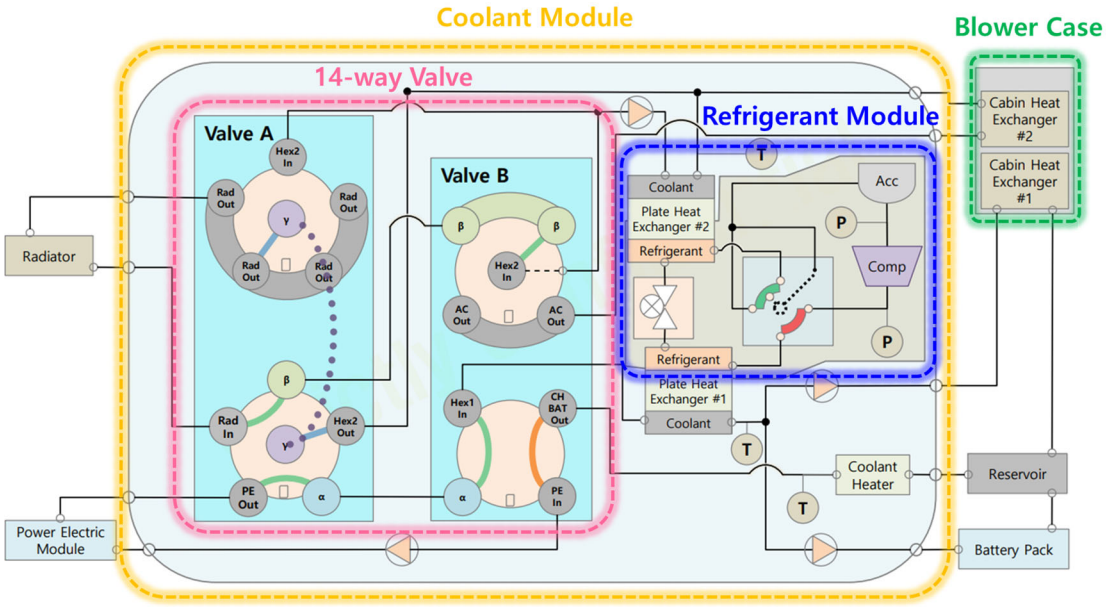

Figure 2. The schematic diagram of the 14-way valve-based ITMS.

The refrigerant module located in the center consists of a compressor, two plate heat exchangers, and an electronic expansion valve, facilitating the smooth absorption and release of heat from the coolant.

The coolant module consists of four water pumps, a coolant heater, and a 14-way valve. The working fluid used is a mixture of coolant (water: ethylene glycol = 50:50) [49]. Based on the operation of the water pumps and the 14-way valve, heat exchange is performed between the refrigerant system, coolant module, and blower case.

The blower case mixes internal and external air through the blower, then passes it through cabin heat exchangers #1 and #2. This heated or cooled air is delivered to the cabin, ensuring passenger comfort.

2.2.2. Coolant System Modeling

Electric Water Pump Modeling

The electronic water pump, in conjunction with the 14-way valve, is a key component that determines both the flow rate and direction of the coolant, significantly impacting the ITMS. Therefore, it was modeled using test data on rotational speed and pressure difference. The power consumption can be expressed as follows.

$$P_{ewp} = \dot{m}_{ewp,out} \frac{\left(p_{ewp,in}/\rho_{ewp,in} - p_{ewp,out}/\rho_{ewp,out}\right)}{\eta_{mec}} \quad (6)$$

14-Way Valve Modeling

The 14-way valve is a multi-port valve consisting of two rotating valve modules. Depending on the operating mode, the configured 14-way valve can flexibly determine the inlet and outlet. Thus, the flow direction and flow rate of the coolant are determined based

on the operation of the 14-way valve and the coolant pump, significantly simplifying the length of the coolant flow path. The flow rate of the fluid flowing through the 14-way valve is calculated based on the valve's flow coefficient, as follows.

$$q = A_{orifice} C_q(\lambda) \sqrt{\frac{2|\Delta p|}{\rho_{upstream}}} \tag{7}$$

Here, C_q is the flow coefficient of the variable orifice, and $A_{orifice}$ is calculated as follows for the variable orifice.

$$\begin{gathered} A_{orifice} = A_{max} cmd_{orifice} \\ 0 \leq cmd_{orifice} \leq 1 \end{gathered} \tag{8}$$

2.2.3. HVAC System Modeling

Compressor Modeling

The displacement of the compressor is assumed to be 45 cc/rev, with a volumetric efficiency of 0.7, an isentropic efficiency of 0.75, and a mechanical efficiency of 0.9, which corresponds to the general performance range [50,51]. The mass flow rate of the compressor is calculated as follows.

$$\dot{m}_{comp} = \eta_v \rho_{out} \omega_{comp} V_{comp} \tag{9}$$

The power consumption of the compressor is calculated as follows.

$$P_{comp} = \frac{\dot{m}_{comp} \left(h_{out} - h_{in}\right)}{\eta_{is} \eta_{mec}} \tag{10}$$

Heat Exchanger Modeling

The heat exchange between the two fluids is calculated as follows.

$$\dot{Q}_{hex} = H_1 A_1 \left(T_1 - T_{wall,in}\right) + H_2 A_2 \left(T_2 - T_{wall,out}\right) \tag{11}$$

Here, A_1 and A_2 represent the heat transfer areas, while the heat transfer coefficients H_1 and H_2 are calculated as follows, depending on the condensation and evaporation processes.

$$\begin{gathered} H_{cond} = H_l \left[(1-x)^{0.8} + \left(3.8 \frac{x^{0.76}(1-x)^{0.04}}{(P_{red})^{0.38}}\right)\right] (at\ condensation\ process) \\ H_{evap} = A H_{NcB} + \phi H_{cv}\ (at\ evaporation\ process) \end{gathered} \tag{12}$$

Additionally, the temperature related to the heat transfer area is calculated as follows.

$$\frac{dT_{wall,hex}}{dt} = \frac{\dot{Q}_{hex}}{m_{hex} C_{p,hex}} \tag{13}$$

Cabin Modeling

In this study, the volume of the cabin is assumed to be 3 m^3, and it is assumed that the simulation starts under temperature conditions identical to the ambient temperature.

Heat loss occurs through the contact surface of the cabin walls with the outside air, and the temperature of the walls is calculated by considering the combined effects of solar radiation heat transfer, heat transfer with the internal air, and heat transfer with the external air.

$$\begin{gathered} \frac{dT_{wall,cabin}}{dt} = \frac{\dot{Q}_{solar} + \dot{Q}_{int} + \dot{Q}_{ext}}{m_{wall,cabin} C_{p,wall,cabin}} \\ \dot{Q}_{solar} = \alpha A_{ext} \phi_{solar} \\ \dot{Q}_{int} = h_{int} A_{int} \left(T_{wall,cabin} - T_{cabin}\right) \\ \dot{Q}_{ext} = h_{ext} A_{ext} \left(T_{wall,cabin} - T_{amb}\right) \end{gathered} \tag{14}$$

Here, α is the solar flux absorption coefficient. ϕ_{solar} represents the solar flux, which is assumed to be the standard value of 700 W/m^2 in this study [52,53].

2.3. System Integration

The 1D simulation model introduced in this study was developed using AMESim 2310 software. The model consists of the powertrain system, auxiliary power source, integrated coolant module, HVAC system, and thermal management control logic.

The powertrain system is responsible for the vehicle's driving, fast charging, and thermal load prediction, and for supplying power to the ITMS. Based on the supplied power, the ITMS performs thermal management for the entire vehicle and optimizes thermal management to support the efficient operation of the powertrain system. The integrated plant system is designed to predict the overall thermal load, thermal management performance, energy load, and efficiency of the BEV.

3. Operating Analysis and System Simulation

3.1. Operating Modes of the 14-Way Valve-Based ITMS

The 14-way valve-based ITMS can perform integrated thermal management for BEVs under various environmental conditions. The main operating modes are listed in Table 2, with each mode responding to different thermal load conditions based on the operation of the 14-way valve and refrigerant switch. This paper aims to manage thermal performance for the cabin and electrical components while driving at ambient temperatures of 35 °C and −10 °C, and to evaluate the concentrated thermal management performance for the battery during fast charging. Therefore, this study utilizes key thermal management modes: modes 1, 4, 12, 13, and 14.

Table 2. Operating modes of the 14-way based ITMS (*: applied in this paper).

Mode No.	Description	Valve Operation Mode		
		Valve A	Valve B	Refrigerant Switch
*1	Air source heating	1	1	1
2	Inefficient heating	3	1	1
3	Inefficient heating and refrigerant drying	3	1	3
*4	Waste heat recovery heating	4	3	2
5	External air heat absorption and electrical component warm-up	1	1	1
6	Inefficient electrical component warm-up	3	1	1
7	Inefficient electrical component warm-up and refrigerant drying	3	1	3
8	Battery thermal storage	2	2	1
9	Defogging	4	3	2
10	Defrost	4	3	2
11	Dehumidification	2	2	2
*12	Battery charging and cooling	5	4	2
*13	Battery and cabin cooling	5	4	2
*14	PE warm-up and cabin cooling	3	4	2

When the BEV is driven in hot climate conditions at 35 °C, it uses the 14th thermal management mode shown in Figure 3e to transfer heat absorbed from the HVB and the cabin at Plate HEX #1 to Plate HEX #2, thereby heating the PE module. If the PE module overheats, the heat from the coolant loop on the Plate HEX #1 side is absorbed by the refrigerant system through the 13th thermal management mode shown in Figure 3d and released into the coolant loop on the Plate HEX #2 side, ultimately being discharged through the radiator.

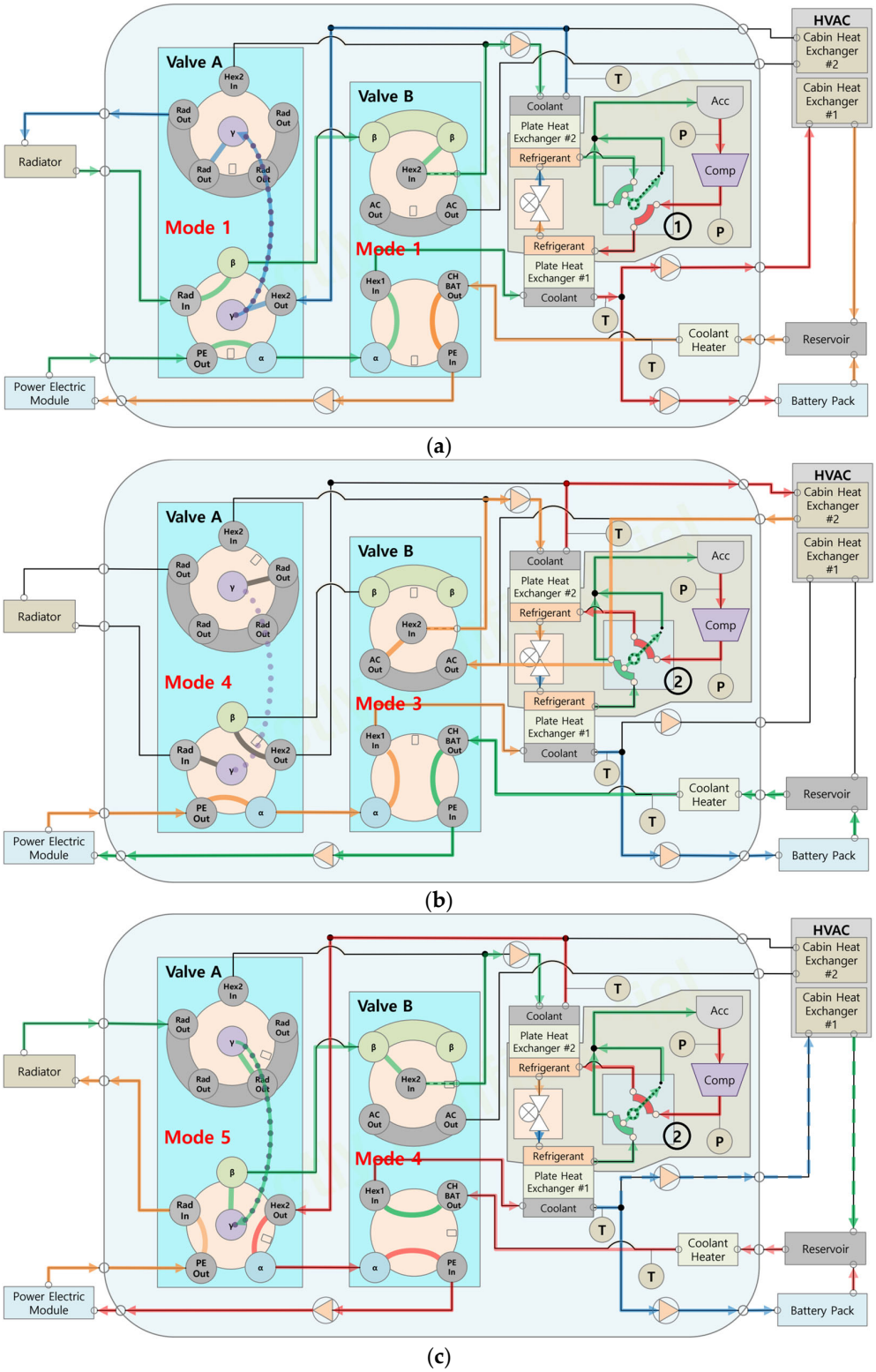

Figure 3. *Cont.*

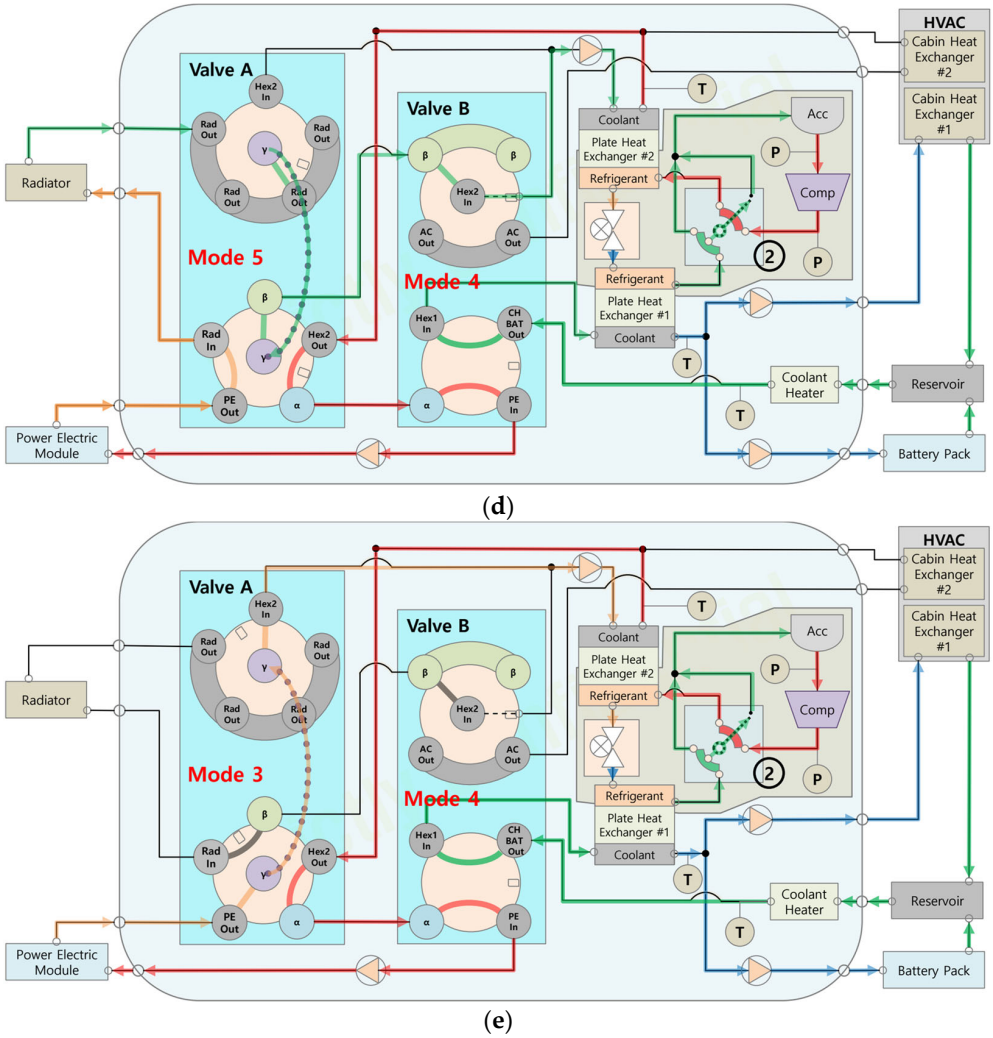

Figure 3. Operating modes of the 14-way valve-based ITMS. (**a**) Mode 1: Air source heating. (**b**) Mode 4: Waste heat recovery heating. (**c**) Mode 12: Battery charging and cooling. (**d**) Mode 13: Battery and cabin cooling. (**e**) Mode 14: PE warm-up and cabin cooling.

Conversely, when driving in cold climate conditions at −10 °C, the first thermal management mode shown in Figure 3a is utilized to cool the coolant loop on the Plate HEX #2 side to a temperature lower than the outside air, thereby absorbing heat from the outside air at the radiator. This heat is then transferred to Plate HEX #1 to warm the cabin and electrical components. If the HVB overheats, the thermal management mode is switched to the fourth mode in Figure 3b, which retrieves heat from the HVB and PE module to efficiently heat the cabin.

Additionally, when concentrated cooling of the HVB is required during fast charging, the 12th thermal management mode shown in Figure 3c is used. This mode absorbs heat from the coolant loop on the Plate HEX #1 side through the refrigerant system and utilizes it for heating the PE module while simultaneously discharging heat to the outside through the radiator.

3.2. Control Strategy for 14-Way Valve-Based ITMS

The control strategy developed in this study determines the efficient operating mode based on the temperatures of the HVB, cabin, and electrical components, as well as the operating conditions. First, it identifies whether the BEV is in charging mode during startup. If it is not charging, the thermal management strategy for the cabin is prioritized based on the ambient temperature and the target cabin temperature. When the ambient temperature

is higher, the system selects either the 13th or 14th thermal management mode for cabin cooling, adjusting the mode based on the temperature of the PE module. Conversely, if the ambient temperature is lower, it selects either the first or fourth thermal management mode for cabin heating, adjusting the mode based on the temperature of the HVB. If the BEV is charging, the thermal management mode is selected based on the ambient temperature and the temperature of the HVB. If the HVB temperature is low and rapid heating is required, the 1st thermal management mode is used, while the 12th thermal management mode is used if cooling is necessary. This control strategy ensures the safety of the system and prevents overload of the ITMS. Consequently, the threshold-based control strategy applied in this study is illustrated in Figure 4.

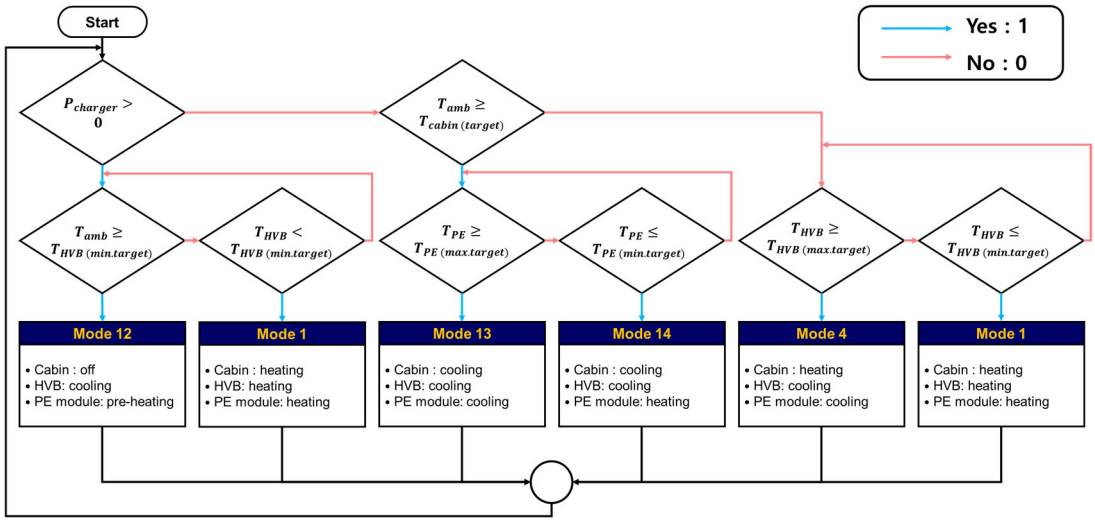

Figure 4. Threshold-based control strategy flowchart for the 14-way valve-based ITMS.

4. Results and Discussion

4.1. Operating Conditions

The developed BEV system is intended to be evaluated under common high- and low-temperature environments encountered during actual operation. For this purpose, it will be assessed in a total of four cases, high-temperature driving, low-temperature driving, high-temperature fast charging, and low-temperature fast charging, as shown in Table 3. During the driving conditions, the vehicle will follow four WLTP class 3 [54–56] driving cycles for a duration of 7200 s, as illustrated in Figure 5. The WLTP class 3 driving cycle is divided into four speed ranges, low, medium, high, and extra high, and consists of patterns that simulate driving in urban and suburban areas. Under fast charging conditions, the HVB will be charged from 10% to 90%.

Table 3. Parameters by operating conditions.

Simulation Cases	Ambient Temperature [°C]	Ambient Relative Humidity [%]	Initial HVB SOC [%]
Hot climate driving	35	60	90
Cold climate driving	−10	40	90
Hot climate fast charging	35	60	10
Cold climate fast charging	−10	40	10

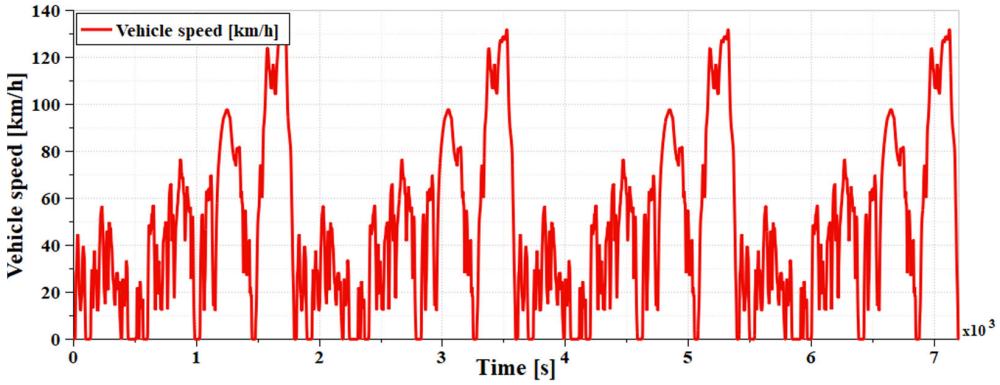

Figure 5. WLTP class 3 driving cycle tracking results.

During driving, the cabin, with passengers on board, is controlled to maintain a temperature of 23 °C and relative humidity of 50–60% in hot climates, and 21 °C and relative humidity of 40–50% in cold climates. This ensures that the comfort zone as specified by ASHRAE Standard 55 [25] and ISO 7730 [26] is fully met, guaranteeing thermal comfort for the passengers. The HVB is controlled to operate within a stable range of 15–40 °C during both driving and charging conditions [14]. The optimal operating temperature range for the PE module is −40 to 90 °C, and it is maintained within this appropriate range depending on the operation of the thermal management system [24].

4.2. Simulation Case 1: Hot Climate Driving

In these conditions, the vehicle was tested using the WLTP driving cycle at an ambient temperature of 35 °C. During cold starts, the BEV must remove a significant amount of heat to cool the cabin and electrical components. By increasing the temperature of the condenser heat source, heat can be effectively released to the outside through the radiator. Therefore, the 14th thermal management mode shown in Figure 3e was used to quickly heat the temperature of the PE module, a component of the condenser heat source, as illustrated in Figure 6. Subsequently, if the temperature of the PE module exceeds 45 °C, the 13th thermal management mode shown in Figure 3d is activated to discharge heat from the condenser heat source to the outside air via the radiator.

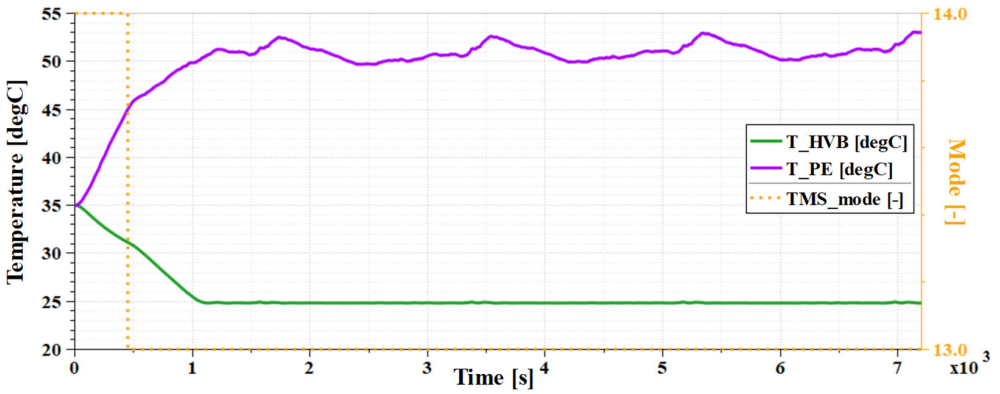

Figure 6. Temperature of BEV components (at hot climate driving).

The HVB also maintained an appropriate temperature range through eWP #2, and the air entering the cabin was cooled via cabin heat exchanger #1, ensuring passenger comfort, as shown in Figure 7. As indicated in Figure 8, the power consumption of the ITMS initially increased to 4–5 kW due to the high cooling load. Subsequently, as the temperatures of the HVB, cabin, and condenser heat source stabilized and the cooling load decreased, the power consumption was reduced to a stable level of 2–3 kW, effectively managing the thermal conditions for the HVB, PE module, and cabin.

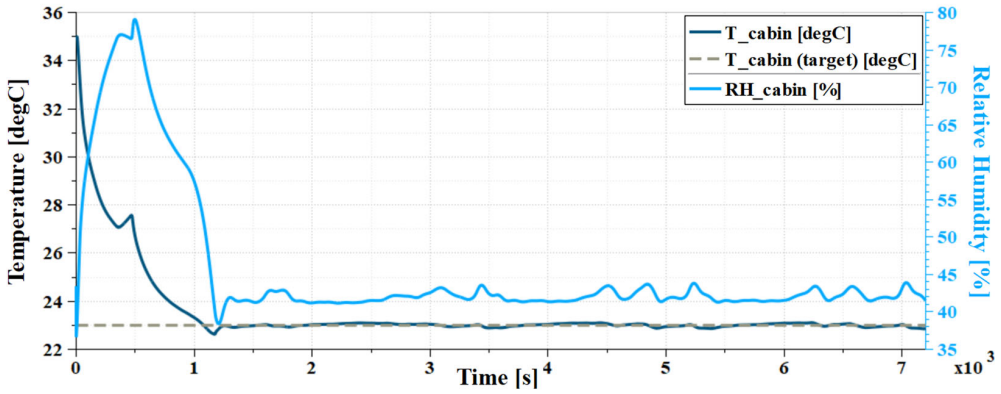

Figure 7. Cabin temperature and relative humidity (at hot climate driving).

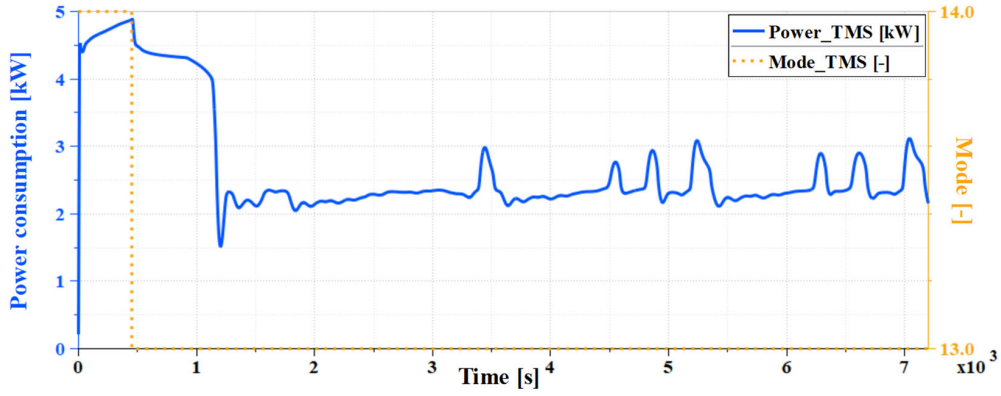

Figure 8. Power consumption of the ITMS (at hot climate driving).

As a result, the electric efficiency increased to 4.82 km/kWh by the end of the driving session, as shown in Figure 9, due to the reduction in power consumption of the ITMS. Considering the total capacity of the HVB at 75 kWh, the ITMS with the 14-way valve is expected to enable a driving range of over 361.5 km during WLTP driving at an ambient temperature of 35 °C.

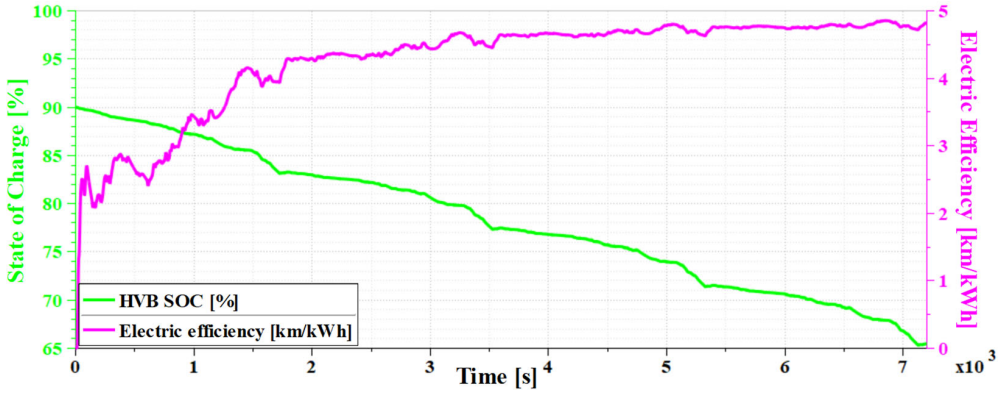

Figure 9. HVB SOC and electric efficiency (at hot climate driving).

4.3. Simulation Case 2: Cold Climate Driving

In this condition, the vehicle was tested using the WLTP driving cycle at an ambient temperature of −10 °C. During cold starts, the BEV requires a significant amount of heat to warm the cabin and electrical components. However, since the heat pump system alone cannot provide sufficient heating capacity, PTC heaters and coolant heaters must be used to

ensure the durability of the electrical components and the thermal comfort of passengers, even considering the increase in power consumption.

During cold starts, the PTC heater and coolant heater are activated, and the first thermal management mode shown in Figure 3a is used to absorb heat from the cold outside air. This heats the HVB and cabin, as shown in Figures 10 and 11. To minimize power consumption, the PTC heater operates only until the cabin temperature reaches 18 °C.

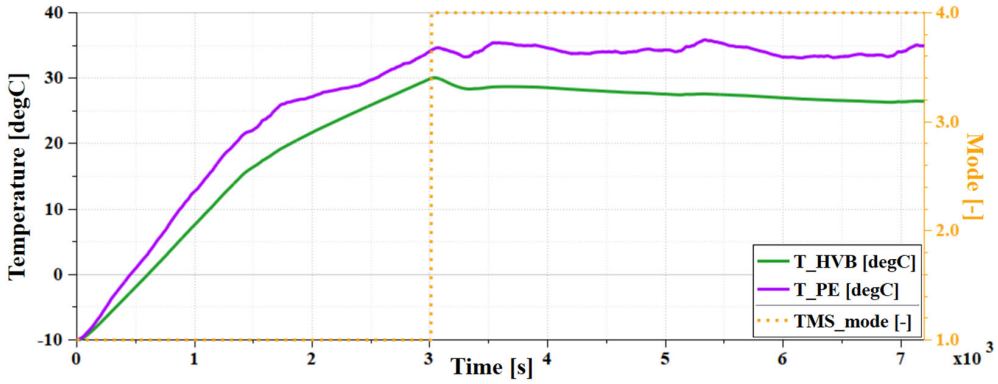

Figure 10. Temperature of BEV components (at cold climate driving).

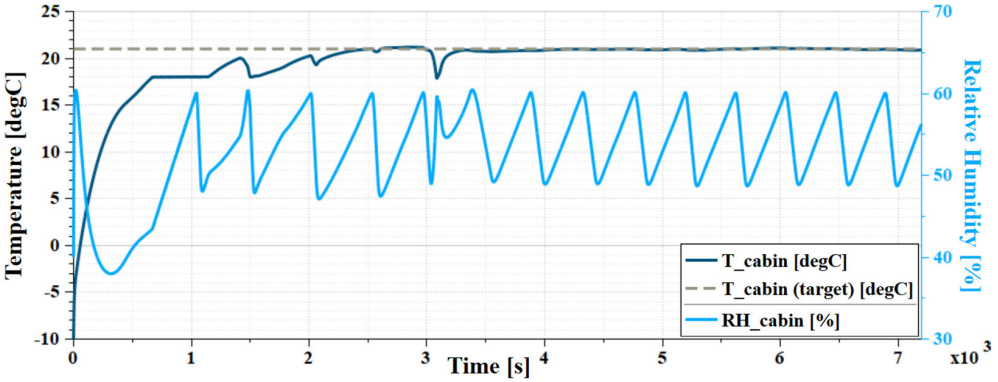

Figure 11. Cabin temperature and relative humidity (at cold climate driving).

As shown in Figures 11 and 12, during the 670 to 1140 s interval, the cabin temperature remains at 19 °C due to the low heating capacity of the heat pump, which is insufficient to heat the cabin adequately. Later, when the heat pump can heat the cabin to the target temperature of 21 °C, the cabin temperature starts to rise. Once the HVB temperature exceeds the appropriate range of 15 °C, the coolant heater stops operating, resulting in a decrease in power consumption observed at the 1400 s mark in Figure 12.

Subsequently, when the HVB temperature rises to 30 °C, the thermal management mode switches to the fourth mode, shown in Figure 3b, to reduce ITMS power consumption. At this point, plate heat exchanger #1 switches from a heating source to a cooling source, while plate heat exchanger #2 switches from a cooling source to a heating source. Additionally, cabin heat exchanger #2, connected to plate heat exchanger #2, provides heating capacity to the cabin. However, until the previously cold coolant is ready to be used for cabin heating, the PTC heater is needed to meet the heating demand, resulting in a temporary increase in power consumption. Later, cabin heating is carried out using waste heat from the electrical components, which allows the ITMS to operate efficiently.

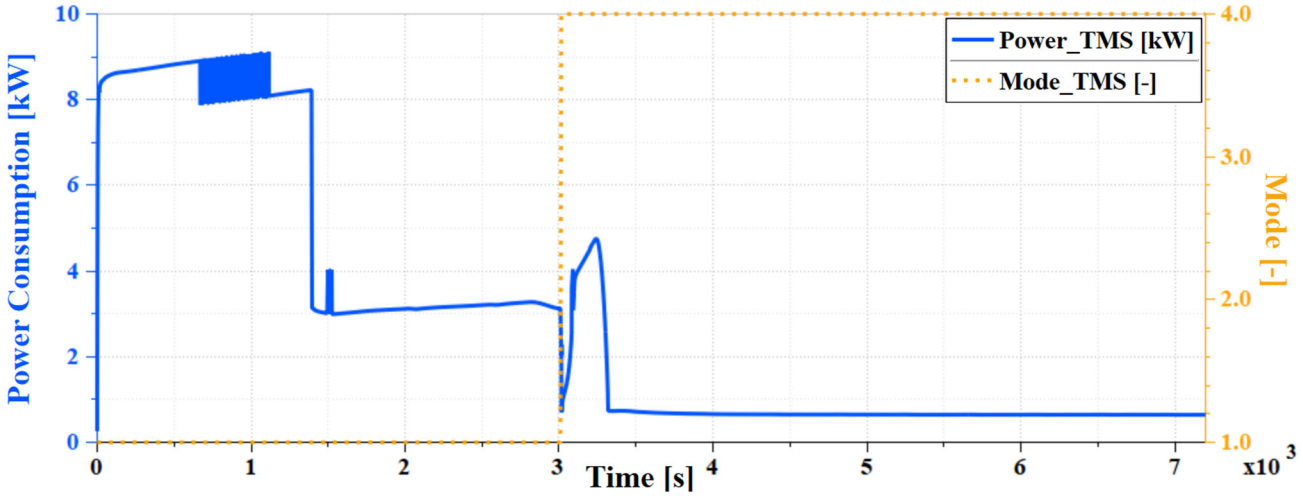

Figure 12. Power consumption of the ITMS (at cold climate driving).

As shown in Figure 13, the electric efficiency increased as the power consumption of the ITMS decreased, ultimately reaching 4.69 km/kWh by the end of the driving session. Considering the total capacity of the HVB at 75 kWh, the ITMS with the 14-way valve is expected to enable a driving range of over 351.8 km during WLTP when driving at an ambient temperature of −10 °C.

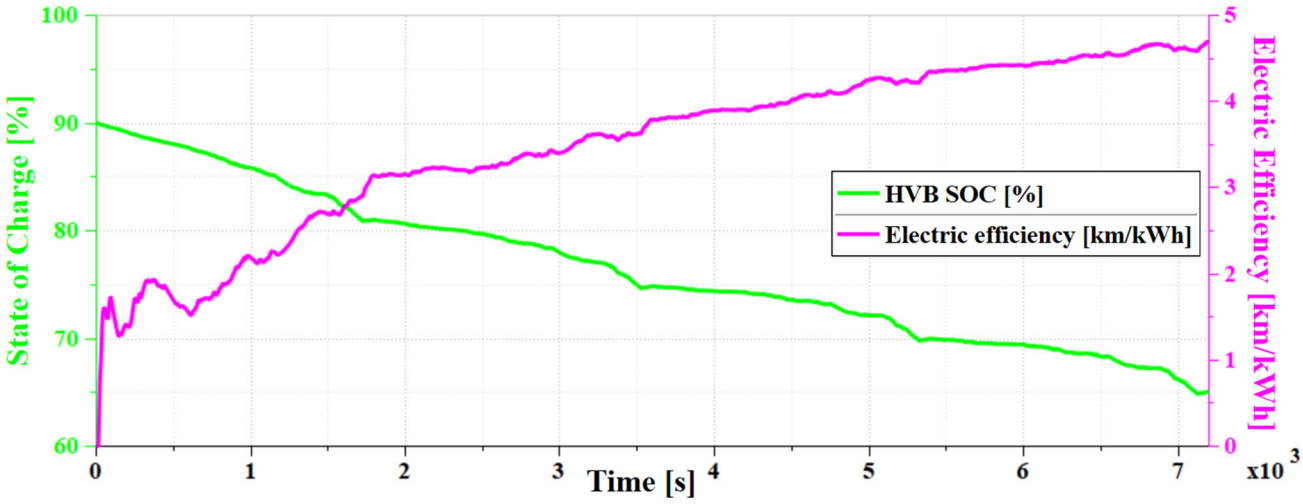

Figure 13. HVB SOC and electric efficiency (at cold climate driving).

4.4. Simulation Case 3: Hot Climate Fast Charging

Under these conditions, a fast charging test of the HVB was conducted at an ambient temperature of 35 °C. During the fast charging test, it was assumed that no passengers were present in the cabin, so no thermal management was performed for the cabin, focusing solely on the thermal management of the HVB. In this case, the 12th thermal management mode, as shown in Figure 3c, was used to cool the HVB.

As shown in Figure 14, the HVB charges a large amount of electrical energy quickly. However, if the HVB overheats, the Battery Management System (BMS) limits the charging power to ensure that the HVB operates within the optimal temperature range, as seen in Figure 15. Additionally, as shown in Figure 16, the ITMS effectively cools the HVB with a low power consumption of approximately 4.2 kW, thus shortening the charging time.

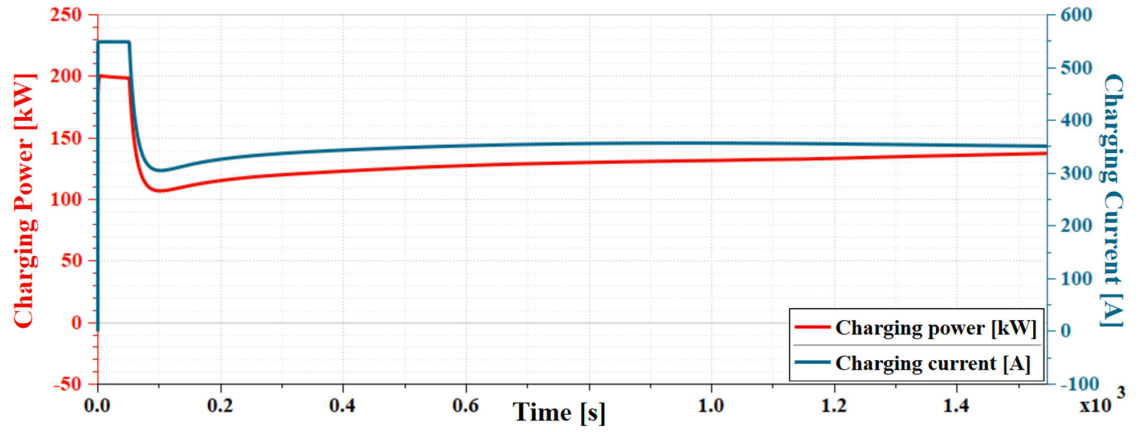

Figure 14. Charging power and current (at hot climate fast charging).

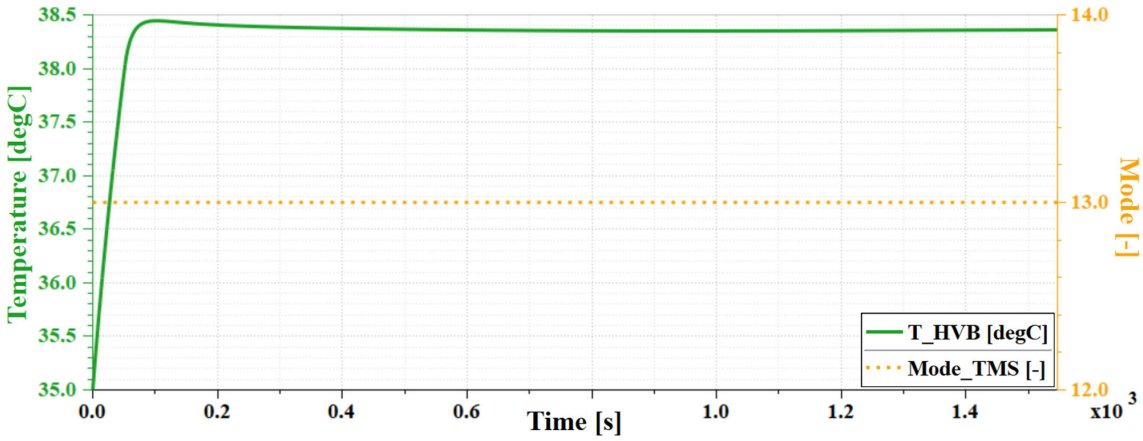

Figure 15. HVB temperature and TMS mode (at hot climate fast charging).

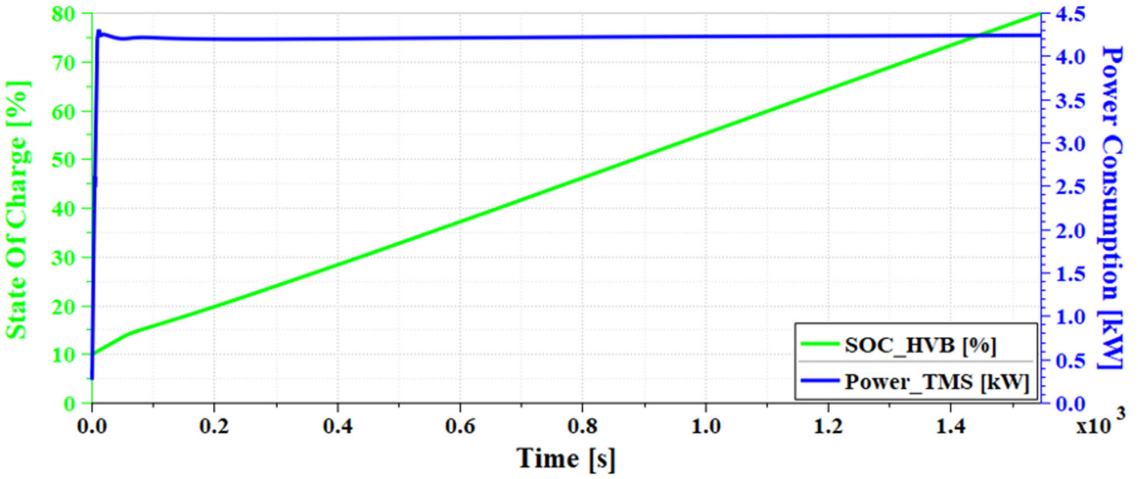

Figure 16. HVB temperature and power losses (at hot climate fast charging).

Consequently, as shown in Figure 16, the ITMS with the 14-way valve is expected to perform fast charging from a 10% to an 80% state of charge (SOC) for the 75kWh HVB within 1546 s under a 35 °C ambient temperature.

4.5. Simulation Case 4: Cold Climate Fast Charging

Under these conditions, a fast charging test of the HVB was conducted at an ambient temperature of −10 °C. Charging at low temperatures can negatively affect the charging

efficiency, performance, and durability of the HVB [57,58]. Therefore, to charge the HVB quickly and safely in a low-temperature environment, an appropriate Battery Management System (BMS) configuration is necessary. The BMS used in this study incrementally increases the charging current according to the operating temperature of the HVB, as shown in Figure 17 [59].

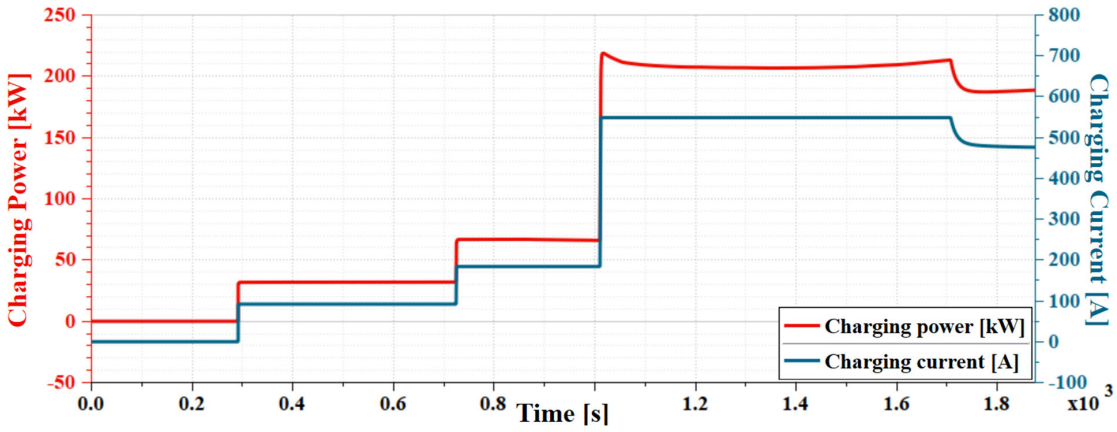

Figure 17. Charging power and current (at cold climate fast charging).

At the start of the simulation, the first thermal management mode shown in Figure 3a is activated to heat the HVB, which is at −10 °C, by absorbing heat from the outside air. Additionally, the coolant heater and heat generated from the charging power are used for the rapid heating of the HVB. Once the HVB reaches its optimal operating temperature of 15 °C, the system switches to the 12th thermal management mode, shown in Figure 3c, focusing on cooling the HVB to perform fast charging efficiently.

Additionally, as shown in Figures 18 and 19, the ITMS requires high power consumption during the initial heating of the HVB. However, after 1010 s, the temperature of the condenser heat source decreases, allowing the HVB to be cooled with lower power consumption, thus shortening the charging time.

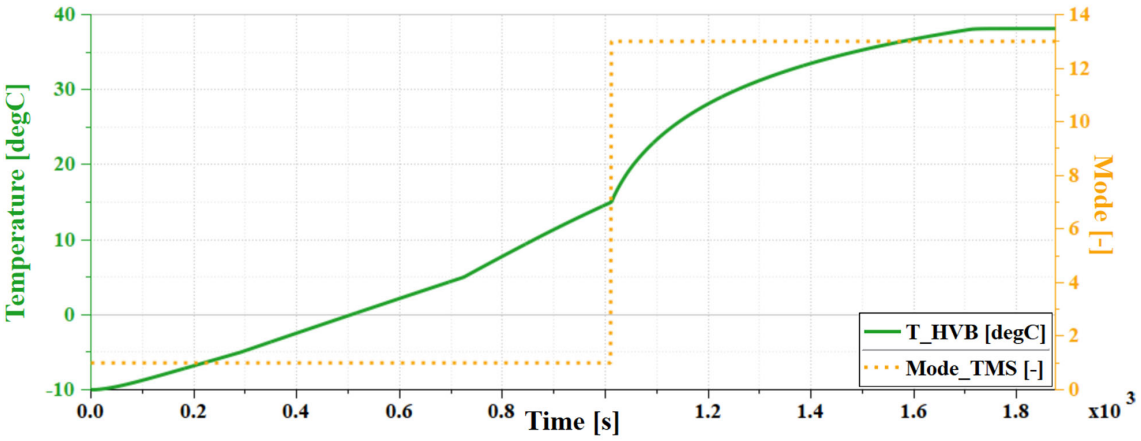

Figure 18. HVB temperature and TMS mode (at cold climate fast charging).

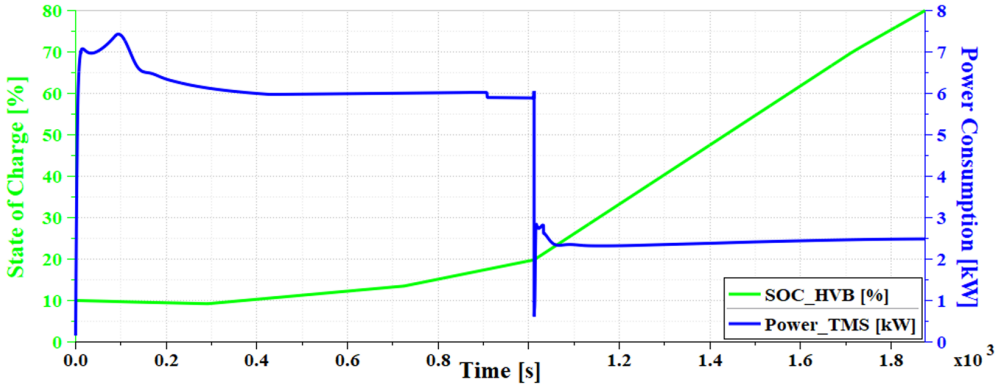

Figure 19. HVB temperature and power losses (at cold climate fast charging).

Consequently, as shown in Figure 19, the ITMS with the 14-way valve is expected to perform fast charging from a 10% to an 80% SOC for the 75 kWh HVB within 1875 s under a −10 °C ambient temperature.

4.6. Summary of Results

The simulation results are summarized in Table 4. The BEV equipped with the 14-way valve-based ITMS showed higher energy consumption in the cold climate of −10 °C compared to the hot climate of 35 °C. However, due to the application of R290 refrigerant, the heat pump system maintained high efficiency even in the cold climate, resulting in only a modest increase in energy consumption compared to the hot climate. Additionally, a Tesla Model Y with the same powertrain specifications and equipped with an Octovalve-ITMS is expected to achieve a driving range of approximately 290 km at ambient temperatures of 35 °C and −10 °C. In contrast, the 14-way valve-based ITMS is expected to achieve a superior driving range of approximately 361.5 km in the hot climate and 351.8 km in the cold climate, demonstrating the potential for significant driving range improvement with the 14-way valve-based ITMS [60].

Table 4. Parameters by operating conditions.

Simulation Cases	Total Energy Consumption of ITMS [kJ]	Final Electric Efficiency [km/kWh]	Charging Time [s]	Estimated Driving Range [km]
Hot climate driving	69,870	4.82	-	361.5
Cold climate driving	70,843	4.69	-	351.8
Hot climate fast charging	6514	-	1546	-
Cold climate fast charging	8.237	-	1875	-

During fast charging, stable and efficient thermal management was achieved together with the configured BMS. Specifically, under the fast charging condition at 35 °C, the 14-way valve-based ITMS achieved a charging time of 1546 s, which is shorter than the 1620 s required by the Octovalve-ITMS-equipped Tesla Model Y under more moderate ambient conditions, highlighting the superior performance of the 14-way valve-based ITMS in fast charging scenarios [61].

5. Conclusions

In this study, a 14-way valve-based ITMS was designed to manage the thermal behavior of a BEV in an integrated manner, to comply with environmental regulations, and to achieve system simplification. The performance was evaluated under various ambient temperatures and operating conditions. As a result, the following conclusions were drawn.

1. The developed 14-way valve-based ITMS increased system stability and reduced complexity by minimizing the number of BEV components and flow path lengths, thus improving overall efficiency and reliability.
2. The 14-way valve system using R290 refrigerant complies with environmental regulations, making it a sustainable choice by reducing the environmental impact and supporting long-term BEV efficiency.
3. This ITMS demonstrated its ability to achieve stable and efficient thermal management when driving the WLTP cycle under both hot and cold climate conditions.
4. The system also provided stable and efficient thermal management during fast charging in both hot and cold environments. By regulating heat effectively, it shortened charging times and helped to prevent battery degradation, which is critical for improving the BEV user experience.

This study presents the potential of an efficient thermal management system that is both environmentally friendly and capable of reducing manufacturing costs. By focusing on the design and evaluation of an ITMS for BEVs at the system level, this study demonstrates how such a system can enhance energy efficiency and increase driving range. While the component-level modeling has been simplified, and certain real-world factors such as continuous driving conditions, post-driving charging, flame propagation, and corrosion have not been fully accounted for, the results show promise for improving BEV performance. To address these limitations, future research will focus on optimizing the model to incorporate a broader range of operational conditions and performing field tests within a Hardware-in-the-Loop Simulation environment to validate the ITMS's reliability and functionality. Additionally, we plan to explore cost optimization at the vehicle level to enhance overall system practicality. This system is not only expected to improve BEV energy efficiency but is also positioned to play a key role in optimizing the design and production processes of future BEVs, contributing to a more sustainable and cost-effective approach in electric vehicle technology.

Author Contributions: Conceptualization: J.B.; investigation: J.B. and J.Y.; writing—original draft preparation: J.B., J.Y. and J.H.; writing—review and editing: J.Y. and J.H.; and supervision: J.Y. and J.H. All authors have read and agreed to the published version of the manuscript.

Funding: This research was financially supported by the Ministry of Trade, Industry, and Energy (MOTIE), Korea, under the "Project for Research and Development with Middle Markets Enterprises and DNA (Data, Network, AI) Universities" (Development of Integrated Electric Vehicle Thermal Management System Operation Strategy and Efficiency Improvement Technology Using Neural Network-based MRAC Technique) (reference number P0024561) supervised by the Korea Institute for Advancement of Technology (KIAT). This research was supported by "Regional Innovation Strategy (RIS)" through the National Research Foundation of Korea (NRF) funded by the Ministry of Education (MOE) (2023RIS-007).

Data Availability Statement: Data are contained within the article.

Conflicts of Interest: The authors declare no conflicts of interest.

Nomenclature

A	Area [m^2]
C_p	Specific heat [J/kg·K]
C_q	Flow coefficient [-]
h	Specific enthalpy [J/kg]
H	Convective heat transfer coefficient [$W/m^2 \cdot K$]
I	Current [A]
m	Mass [kg]
m	Mass flow rate [kg/s]
P	Power [kW]
p	Pressure [kPa]

q	Volume flow rate [m^3/s]
Q	Heat transfer rate [kW]
R	Resistance [ohm]
T	Temperature [°C]
t	Time [s]
V	Volume [m^3]
x	Quality [-]
Subscripts and superscripts	
amb	Ambient
cabin	Cabin
case	Case
cell	Cell
cmd	Command
comp	Compressor
con	Condenser
cond	Conduction
conv	Convection
converter	Converter
cool	Coolant
cv	Convective boiling
elec	Electrical
eva	Evaporator
ewp	Electric water pump
ext	External
hex	Heat exchanger
in	Inlet
int	Internal
inverter	Inverter
is	Isentropic
l	Liquid
max	Maximum
mec	Mechanical
motor	Motor
NB	Nucleate boiling
out	Outlet
orifice	Orifice
solar	Solar
upstream	Upstream
v	Volumetric
wall	Wall
Greek	
α	Absorption coefficient [-]
ϕ	Heat flux [W/m^2]
ρ	Density [kg/m^3]
ω	Rotational speed [RPM]
η	Efficiency [-]

References

1. European Commission. Available online: https://ec.europa.eu/commission/presscorner/detail/en/ip_21_3541 (accessed on 14 July 2021).
2. NHTSA. Available online: https://www.nhtsa.gov/laws-regulations/corporate-average-fuel-economy (accessed on 7 June 2024).
3. Grunditz, E.A.; Thiringer, T. Characterizing bev powertrain energy consumption, efficiency, and range during official and drive cycles from gothenburg, sweden. *IEEE Trans. Veh. Technol.* **2015**, *65*, 3964–3980. [CrossRef]
4. Åhman, M. Primary energy efficiency of alternative powertrains in vehicles. *Energy* **2001**, *26*, 973–989. [CrossRef]
5. Woo, J.; Magee, C.L. Forecasting the value of battery electric vehicles compared to internal combustion engine vehicles: The influence of driving range and battery technology. *Int. J. Energy Res.* **2020**, *44*, 6483–6501. [CrossRef]
6. Tran, M.K.; Bhatti, A.; Vrolyk, R.; Wong, D.; Panchal, S.; Fowler, M.; Fraser, R. A review of range extenders in battery electric vehicles: Current progress and future perspectives. *World Electr. Veh. J.* **2021**, *12*, 54. [CrossRef]

7. Kölbl, R.; Bauer, D.; Rudloff, C. Travel behavior and electric mobility in Germany: Is the problem the driving range, costs, or both? *Transp. Res. Rec.* **2013**, *2385*, 45–52. [CrossRef]
8. Reiter, C.; Wassiliadis, N.; Wildfeuer, L.; Wurster, T.; Lienkamp, M. Range extension of electric vehicles through improved battery capacity utilization: Potentials, risks and strategies. In Proceedings of the 2018 21st International Conference on Intelligent Transportation Systems (ITSC), Maui, HI, USA, 4–7 November 2018; pp. 321–326.
9. Yang, C. Running battery electric vehicles with extended range: Coupling cost and energy analysis. *Appl. Energy* **2022**, *306*, 118116. [CrossRef]
10. Recurrent. Available online: https://www.recurrentauto.com/research/winter-ev-range-loss (accessed on 2 January 2024).
11. Pizzonia, F.; Castiglione, T.; Bova, S. A Robust Model Predictive Control for efficient thermal management of internal combustion engines. *Appl. Energy* **2016**, *169*, 555–566. [CrossRef]
12. Chalet, D.; Lesage, M.; Cormerais, M.; Marimbordes, T. Nodal modelling for advanced thermal-management of internal combustion engine. *Appl. Energy* **2017**, *190*, 99–113. [CrossRef]
13. Hamdy, M.; Askalany, A.A.; Harby, K.; Kora, N. An overview on adsorption cooling systems powered by waste heat from internal combustion engine. *Renew. Sustain. Energy Rev.* **2015**, *51*, 1223–1234. [CrossRef]
14. Liu, S.; Liu, X.; Dou, R.; Zhou, W.; Wen, Z.; Liu, L. Experimental and simulation study on thermal characteristics of 18,650 lithium–iron–phosphate battery with and without spot–welding tabs. *Appl. Therm. Eng.* **2020**, *166*, 114648. [CrossRef]
15. Wang, F.; Lin, Z.; Liu, L.; Wei, X.; Lin, S.; Dai, L.; Wei, Y.; Liang, C.; Liaw, B.Y. Does Polarization Increase Lead to Capacity Fade? *J. Electrochem. Soc.* **2020**, *167*, 090549. [CrossRef]
16. Aris, A.M.; Shabani, B. An Experimental Study of a Lithium Ion Cell Operation at Low Temperature Conditions. *Energy Procedia* **2017**, *110*, 128–135. [CrossRef]
17. Łebkowski, A. Temperature, Overcharge and Short-Circuit Studies of Batteries used in Electric Vehicles. *Prz. Elektrotech.* **2017**, *93*, 67–73. [CrossRef]
18. Sun, P.; Bisschop, R.; Niu, H.; Huang, X. *A Review of Battery Fires in Electric Vehicles*; Springer: New York, NY, USA, 2020; pp. 1–50.
19. Petzl, M.; Kasper, M.; Danzer, M.A. Lithium plating in a commercial lithium-ion battery—A low-temperature aging study. *J. Power Sources* **2015**, *275*, 799–807. [CrossRef]
20. Bodenes, L.; Naturel, R.; Martinez, H.; Dedryvère, R.; Menetrier, M.; Croguennec, L.; Pérès, J.-P.; Tessier, C.; Fischer, F. Lithium secondary batteries working at very high temperature: Capacity fade and understanding of aging mechanisms. *J. Power Sources* **2013**, *236*, 265–275. [CrossRef]
21. Song, H.; Cao, Z.; Chen, X.; Lu, H.; Jia, M.; Zhang, Z.; Lai, Y.; Li, J.; Liu, Y. Capacity fade of LiFePO4/graphite cell at elevated temperature. *J. Solid State Electrochem.* **2013**, *17*, 599–605. [CrossRef]
22. Abada, S.; Petit, M.; Lecocq, A.; Marlair, G.; Sauvant-Moynot, V.; Huet, F. Combined experimental and modeling approaches of the thermal runaway of fresh and aged lithium-ion batteries. *J. Power Sources* **2018**, *399*, 264–273. [CrossRef]
23. Ren, D.; Hsu, H.; Li, R.; Feng, X.; Guo, D.; Han, X.; Lu, L.; He, X.; Gao, S.; Hou, J.; et al. A comparative investigation of aging effects on thermal runaway behavior of lithium-ion batteries. *eTransportation* **2019**, *2*, 100034. [CrossRef]
24. Sun, Y.; Zhang, S.; Chen, G.; Tang, Y.; Liang, F. Experimental and numerical investigation on a novel heat pipe based cooling strategy for permanent magnet synchronous motors. *Appl. Therm. Eng.* **2020**, *170*, 114970. [CrossRef]
25. ASHRAE. Thermal environmental conditions for human occupancy. *ANSI/ASHRAE* **1992**, *55*, 5.
26. Alahmer, A.; Omar, M. Vehicular cabins' thermal comfort zones; fanger and berkley modeling. *Veh. Eng.* **2013**, *1*, 19–32.
27. EPA. Available online: https://www.epa.gov/ghgemissions/understanding-global-warming-potentials (accessed on 8 August 2024).
28. EPA. Available online: https://www.epa.gov/pfas/pfas-explained (accessed on 3 October 2024).
29. ATMOsphere. Available online: https://atmosphere.cool/fact_sheets/refrigerants-real-gwp-and-pfas/ (accessed on 11 November 2024).
30. Li, W.; Liu, R.; Liu, Y.; Wang, D.; Shi, J.; Chen, J. Performance evaluation of R1234yf heat pump system for an electric vehicle in cold climate. *Int. J. Refrig.* **2020**, *115*, 117–125. [CrossRef]
31. Huang, Y.; Wu, X.; Jing, J. Research on the electric vehicle heat pump air conditioning system based on R290 refrigerant. *Energy Rep.* **2022**, *8*, 447–455. [CrossRef]
32. Eisele, M. Transient Performance Evaluation of Automotive Secondary Loop Systems. Ph.D. Thesis, University of Maryland, College Park, MD, USA, 2012.
33. Yibiao, W.A.N.G.; Junqi, D.O.N.G.; Shiwei, J.I.A.; Huang, L. Experimental comparison of R744 and R134a heat pump systems for electric vehicle application. *Int. J. Refrig.* **2021**, *121*, 10–22.
34. Wang, M.; Teng, S.; Xi, H.; Li, Y. Cooling performance optimization of air-cooled battery thermal management system. *Appl. Therm. Eng.* **2021**, *195*, 117242. [CrossRef]
35. Akbarzadeh, M.; Kalogiannis, T.; Jaguemont, J.; Jin, L.; Behi, H.; Karimi, D.; Beheshti, H.; Van Mierlo, J.; Berecibar, M. A comparative study between air cooling and liquid cooling thermal management systems for a high-energy lithium-ion battery module. *Appl. Therm. Eng.* **2021**, *198*, 117503. [CrossRef]
36. Shen, M.; Gao, Q. System simulation on refrigerant-based battery thermal management technology for electric vehicles. *Energy Convers. Manag.* **2020**, *203*, 112176. [CrossRef]
37. Singirikonda, S.; Obulesu, Y.P. Adaptive secondary loop liquid cooling with refrigerant cabin active thermal management system for electric vehicle. *J. Energy Storage* **2022**, *50*, 104624. [CrossRef]

38. Leighton, D. *Combined Fluid Loop Thermal Management for Electric Drive Vehicle Range Improvement*; No. NREL/CP-5400-63430; National Renewable Energy Lab. (NREL): Golden, CO, USA, 2015; Volume 8.
39. Tian, Z.; Gu, B.; Gao, W.; Zhang, Y. Performance evaluation of an electric vehicle thermal management system with waste heat recovery. *Appl. Therm. Eng.* **2020**, *169*, 114976. [CrossRef]
40. Shelly, T.; Weibel, J.A.; Ziviani, D.; Groll, E.A. A dynamic co-simulation framework for the analysis of battery electric vehicle thermal management systems. In Proceedings of the 2022 21st IEEE Intersociety Conference on Thermal and Thermomechanical Phenomena in Electronic Systems (iTherm), San Diego, CA, USA, 31 May–3 June 2022; pp. 1–8.
41. Guo, R.; Li, L.; Sun, Z.; Xue, X. An integrated thermal management strategy for cabin and battery heating in range-extended electric vehicles under low-temperature conditions. *Appl. Therm. Eng.* **2023**, *228*, 120502. [CrossRef]
42. Mancini, N.; Stratford, J.; Mardall, M.; Kopitz, J.; O'Donnell, C.R.; Hanks, D.F.; Li, H. Optimal Source Electric Vehicle Heat Pump with Extreme Temperature Heating Capability and Efficient Thermal Preconditioning. Available online: https://patents.google.com/patent/US20190070924A1/en (accessed on 1 November 2021).
43. Wray, A.; Ebrahimi, K. Octovalve thermal management control for electric vehicle. *Energies* **2022**, *15*, 6118. [CrossRef]
44. Bernardi, D.; Pawlikowski, E.; Newman, J. A general energy balance for battery systems. *J. Electrochem. Soc.* **1985**, *132*, 5. [CrossRef]
45. Wang, Y.; Li, J.; Tao, Q.; Bargal, M.H.; Yu, M.; Yuan, X.; Su, C. Thermal management system modeling and simulation of a full-powered fuel cell vehicle. *J. Energy Resour. Technol.* **2020**, *142*, 061304. [CrossRef]
46. Barcellona, S.; Colnago, S.; Dotelli, G.; Latorrata, S.; Piegari, L. Aging effect on the variation of Li-ion battery resistance as function of temperature and state of charge. *J. Energy Storage* **2022**, *50*, 104658. [CrossRef]
47. Mahmud, A.H.; Daud, Z.H.C.; Asus, Z. The impact of battery operating temperature and state of charge on the lithium-ion battery internal resistance. *J. Mek.* **2018**, *40*, 1–8.
48. Li, D.; Zhang, C.; Fan, R.; Xu, L.; Wang, Y.; Guo, W.; Chen, J.; Ni, M. An innovative thermal management method for cooling loop of electric driving system for durable and high efficiency electric vehicle. *Appl. Therm. Eng.* **2021**, *195*, 117176. [CrossRef]
49. Vikram, S.; Vashisht, S.; Rakshit, D. Performance analysis of liquid-based battery thermal management system for Electric Vehicles during discharge under drive cycles. *J. Energy Storage* **2022**, *55*, 105737. [CrossRef]
50. Guth, T.; Atakan, B. Semi-empirical model of a variable speed scroll compressor for R-290 with the focus on compressor efficiencies and transferability. *Int. J. Refrig.* **2023**, *146*, 483–499. [CrossRef]
51. Navarro, E.; Urchueguía, J.F.; Corberán, J.M.; Granryd, E. Performance analysis of a series of hermetic reciprocating compressors working with R290 (propane) and R407C. *Int. J. Refrig.* **2007**, *30*, 1244–1253. [CrossRef]
52. Hossini, N. Evaluation of solar radiation for the use of photovoltaic panels in Afghanistan. *Int. J. Innov. Res. Sci. Stud.* **2021**, *4*, 139–146. [CrossRef]
53. Okasha, A.M. Determination of Critical Irradiance and Overall Efficiency to Lift Water by Solar Energy System. *Misr J. Agric. Eng.* **2017**, *34*, 599–616. [CrossRef]
54. Mock, P.; Kühlwein, J.; Tietge, U.; Franco, V.; Bandivadekar, A.; German, J. The WLTP: How a new test procedure for cars will affect fuel consumption values in the EU. *Int. Counc. Clean Transp.* **2014**, *9*, 1–20.
55. UNECE. Available online: https://unece.org/press/unece-adopts-more-accurate-fuel-efficiency-and-co2-test-new-cars-wltp (accessed on 11 March 2014).
56. DieselNet. Available online: https://dieselnet.com/standards/cycles/wltp.php (accessed on 11 November 2024).
57. Lei, Z.; Zhang, C.; Li, J.; Fan, G.; Lin, Z. Preheating method of lithium-ion batteries in an electric vehicle. *J. Mod. Power Syst. Clean Energy* **2015**, *3*, 289–296. [CrossRef]
58. Wu, S.; Xiong, R.; Li, H.; Nian, V.; Ma, S. The state of the art on preheating lithium-ion batteries in cold weather. *J. Energy Storage* **2020**, *27*, 101059. [CrossRef]
59. Ye, Z.; Fu, X.; Zhou, S. Research on control strategy of rapid preheating for power battery in electric vehicle at low temperatures. *Appl. Therm. Eng.* **2024**, *245*, 122770. [CrossRef]
60. Cars.com. Available online: https://www.cars.com/articles/our-tesla-model-y-in-cold-weather-how-was-range-affected-448043/ (accessed on 20 January 2023).
61. EVBox. Available online: https://evbox.com/en/electric-cars/tesla/tesla-model-y (accessed on 11 November 2024).